

INTERIOR FLOW SIMULATION OF SUCTION CHAMBERS FOR HLFC PROFILES

H. Lüdeke,
DLR, Institut für Aerodynamik und Strömungstechnik,
Lilienthalplatz 7, 38108 Braunschweig, Germany

Abstract

For a simplified but effective suction chamber concept for hybrid laminar flow control by boundary-layer suction, which is investigated on a vertical tail, the velocity distribution inside suction chambers is simulated. Within the current study, CFD simulations of the flow inside these chambers are carried out by the DLR FLOWer code to predict this velocity as well as the pressure distribution inside the chambers. Variations of the suction pressure and the tap-distance are carried out.

1. INTRODUCTION

Within different EU-projects, hybrid laminar flow technology with suction through a porous leading edge of a vertical tail plane (VTP) is investigated by windtunnel tests and numerical analysis by computational fluid dynamics.

The assessment for the integration of an HLFC system into a long range aircraft has to answer the following two questions: How does the integration of an HLFC system into a given long range a/c configuration influences aircraft performance? What is the optimal HLFC aerodynamic and system configuration to obtain maximum performance benefit?

Principal feasibility of HLFC for large transport aircraft was shown for example by Airbus with the flight tests of an HLFC system on the vertical tail plane of an A320 aircraft [1],[2]. The suction systems for these tests were designed to explore the limits of HLFC and were rather complex to explore the envelope of applicability of HLFC. After having shown that HLFC does deliver the aerodynamic results, simpler and lighter systems were developed to obtain the overall benefit for the aircraft. A major step was the simplified suction system developed within the European ALTTA project [3]. This system works without the complex structure of classical systems [4][5] and is currently being refined within the German national project VER²SUS. A numerical investigation of the suction on the boundary layer is carried out in [6].

The concept of an outer porous surface with a sub-structure of stringers and a second inner sheet provides a double-wall shell with a number of integrated suction chambers (FIGURE 1). Inside of these suction chambers given circular orifices allow the choice of an individual pressure to extract enough material and to generate a boundary layer with maximum laminar range. For these chambers the question of constant suction velocities along the outer sheet is crucial, while the flow-field inside these chambers was not investigated in detail up to now. Within the scope of this paper the flow inside these chambers is simulated under simplified assumptions.

The idealization of the geometry allows two dimensional

calculations in cuts through the center plane of the chamber between two respective taps while the rest of the flow is expected periodically repeated (FIGURE 1). The Taps are replaced by slots of the same surface to provide a constant given mass-flow. In the middle between two slots another symmetry plane can be set due to the identical flow in each direction. The suction through the outer sheet is modeled under the assumption of an analytical quadratic relation between pressure-difference over the porous wall and the suction velocity as determined within the ALTTA project [3]. The pressure outside the wall is determined from former calculations and kept constant. Finally the duct inside the orifices is added by the use of a prescribed-pressure boundary condition. Afterwards the velocity distribution along the porous wall inside the chamber as well as the pressure distribution is calculated.

Different configurations of chambers and tap-distances are simulated by inviscid as well as Navier-Stokes simulations.

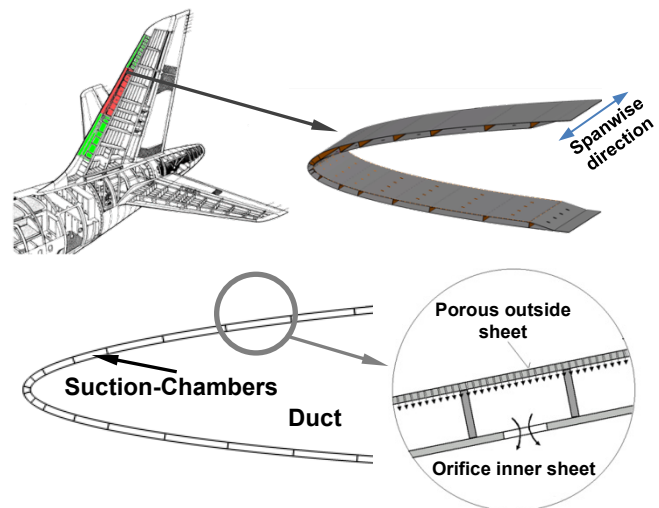


FIGURE 1. Overview of the suction-panel geometry. The sketch of the A320 tail is taken from [3].

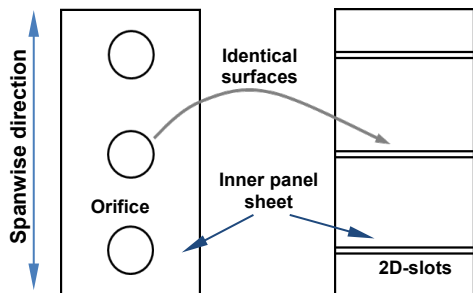


FIGURE 2. Idealization of the circular taps in a spanwise row by slots of identical surface.

2. CONFIGURATION

2.1. Geometry

The concept of an outer porous surface with a sub-structure of stringers and a second inner sheet provides a double-wall shell with a number of integrated suction chambers (FIGURE 1). Inside of the suction chambers drilled circular orifices allow the choice of an individual pressure to extract enough material and to generate a boundary layer on the wing-surface with maximum delay of laminar-turbulent transition. For this study the inner geometry is expected as a rectangular space without any curvature which is nearly infinitely long in spanwise direction. By these assumptions two-dimensional simulations on very simple CFD-grids are possible.

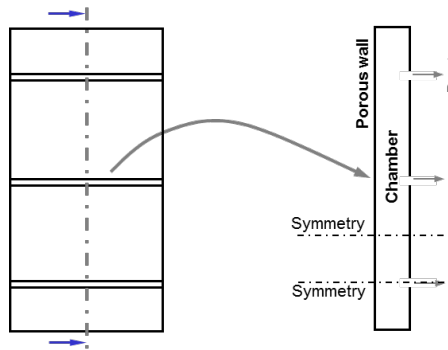


FIGURE 3. Left: top-view of the suction-panel with slots. Right: side-view of the panel with slots and symmetry planes.

2.2. Geometric data

The chambers have generally a rectangular shape with a wall-normal dimension of 10mm, an average chordwise diameter of 100mm and a spanwise length of 2m. Circular orifices with diameters of 3mm are located in a row on the duct-wall (FIGURE 1) along these 2 meters at a distance between 0.125m and 0.25m. So a maximum of 16 equidistant taps appear for each chamber.

In the following, simplifications will be described, that allow 2D calculations between two respective orifices, while the flow is expected perfectly periodic in spanwise direction.

2.3. Idealizations

Various idealizations of the complex flow field as well as the geometry are carried out. The suction velocity is determined by the local pressure loss over the porous sheet only, omitting any influence of single microporosities. The surface pressure at the boundary-layer wall is taken from the simulations of the tail profile and is set as a constant in time and space.

To replace the inherently 3D flow by a 2D approximation the circular orifices are replaced by slots of the same surface as the suction holes (FIGURE 2). This simplification will provide the same material flow as the orifices but can be simulated by a 2D cut through the chamber-centerline (FIGURE 3).

After this simplification, the flow between two slots is expected periodic and symmetric and two symmetry planes are defined: one in the middle between slots and the other just in the middle of the next slot

The duct on the inner side of the orifices is replaced by a coarse farfield-grid with a given exit-pressure, which is provided by the fraction of outer and duct-pressure.

Finally a rectangular domain is calculated between one orifice and the next symmetry plane in spanwise direction and the porous wall, the duct wall and the duct-farfield in wall-normal direction. The flow-field is expected as an infinitely repeated structure all over the spanwise dimension which is justified by the chamber size of 2m.

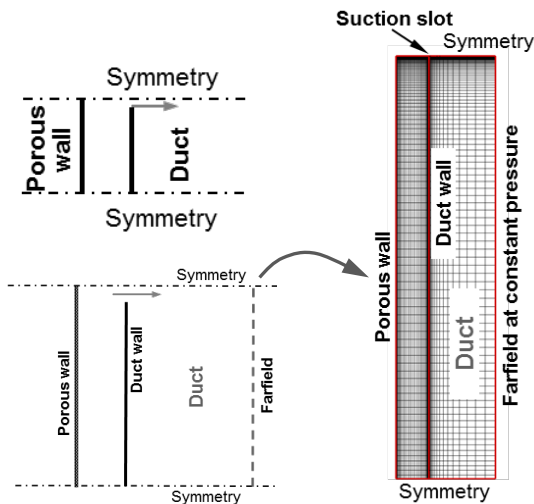


FIGURE 4. Definition of the grid in the duct behind the suction panel.

2.4. CFD grid

Using the formally defined simplifications, a rectangular CFD grid is generated by taking into account strong velocity gradients at the suction slot, near the porous wall, and inside the duct. The Euler mesh is refined near the porous wall to resolve the gradients from the suction velocities.

Navier stokes grids are extensively refined with respect to all walls to resolve the boundary-layer gradients.

Approximately 18 cells are located inside the slot (half-diameter) while 110 cells define the duct-wall. The suction chamber contains 48 cells wall-normal and the Duct-farfield is resolved with 24 cells (FIGURE 5).

The calculations require up to 8 orders of magnitude convergence before a steady flow inside the chamber is reached, similar convergence is required for the duct.

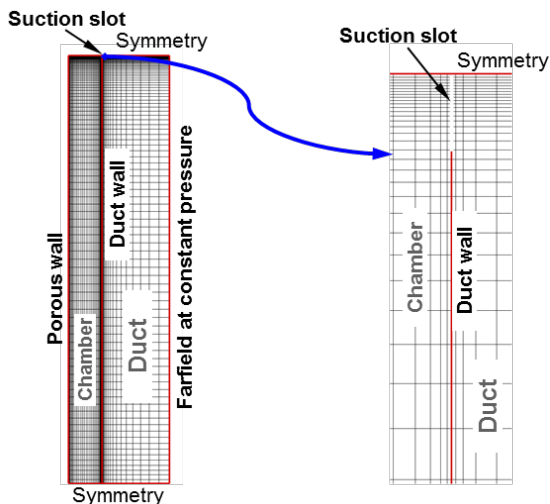


FIGURE 5. Suction panel grid and grid-detail in the slot region.

2.5. Flow conditions

The flow through the suction chamber is defined by the boundary conditions, The Mach-number outside the porous wall and the pressures at the porous wall as well as the pre-scribed duct-pressure. While the pressure outside the porous wall is chosen as a reference value, the duct pressure is given by a ratio between both pressure-values.

To choose a given external pressure for the suction wall of 100500 Pa and a duct-pressure of 99250Pa, the ratio for the code is approx. 0.988.

The reference Mach number of 0.294 is valid outside the porous wall, while inside the duct very small Mach-numbers within a range of 0.01 appear. Even inside the duct very small flow velocities are investigated.

As a first step, inviscid simulations are carried out with slip-walls for the chamber as well as for the duct.

For viscous simulations a reference Reynolds-number per meter of 7 Million is chosen. Due to the very small velocities inside the chamber, the Reynolds-number per meter is about 1400 in the region of interest.

Three Test-cases at different Pressure-values and orifice-distances are defined to provide a small overview of the influences of those parameters (TAB 1).

The relation between suction velocity and pressure difference is taken from the ALTTA experiments and will be described in detail in the next chapter.

Case No.:	$P_{External}$ [Pa]	P_{Duct} [Pa]	L_{Domain} [m]
Case 1	100500	99250	0.125
Case 2	99500	95000	0.125
Case 3	99500	95000	0.0625

TAB 1. Flow conditions and geometry for three different cases.

3. CODE DESCRIPTION

All calculations in this paper were carried out with the DLR FLOWer code [7] by solving the compressible Reynolds-averaged Navier Stokes equations on block-structured grids with second order finite volume techniques and cell-centered variables.

Time advancement is applied by a five-step low-storage second order Runge Kutta method.

Turbulence is modeled by either algebraic or transport equation models. The code is adapted to the simulation of exterior flow fields around complex configurations. Since a rotating reference frame can be used.

The numerical procedure is based on structured meshes, using a central cell-vertex or cell-centered finite volume formulation. Dissipative terms are explicitly added in order to damp high frequency oscillations and to allow sufficiently sharp resolution of shock waves in compressible flow. On smooth meshes, the scheme is second order accurate in space. Time integration is carried out by an explicit hybrid multistage Runge-Kutta scheme. For steady state calculations the integration is accelerated by the techniques of local time stepping, enthalpy damping for inviscid flows and implicit residual smoothing. The solution procedure is embedded into a sophisticated multigrid algorithm which allows standard single grid computations as well as successive grid refinement, with the option of simple or full multigrid.

The code is written in a flexible block structured form enabling treatment of complex aerodynamic configurations with any mesh topology. Two dummy layers around each block are chosen in order to maintain the second order accuracy in space at block intersections.

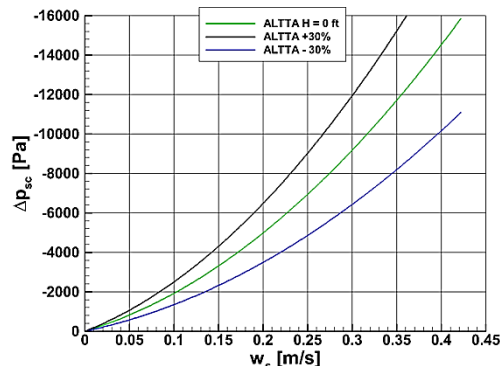


FIGURE 6. Relation of pressure drop and suction velocity across micro-perforated skin: the ALTTA curve.

3.1. Porous-wall boundary condition

The relation between suction velocity and pressure difference is taken from the ALTTA curve (FIGURE 6) where the following empirical formula was found to connect suction-velocity and difference-pressure over the micro-porous wall:

$$\Delta p_{sc} = A \frac{\mu_s}{\mu_0} w_s + B \frac{\rho_s}{\rho_0} w_s^2$$

Where the suction pressure is Δp_{sc} , and w_s is the suction-velocity at the wall.

Due to a very small pressure-difference and suction-velocity ($\Delta p_{sc} < 600 \text{ Pa}$, $w_s < 0.03 \text{ m/s}$) the non-linear part B is omitted.

For the same reason $\mu_s \approx \mu_0$ is expected, so a linearized relation of suction velocity and pressure difference is finally used:

$$\Delta p_{sc} = A \cdot w_s$$

Were A is the slope of the ALTTA-curve (at H=0) near zero-pressure. The dimensional value is calculated from the secant between $0 \frac{\text{m}}{\text{s}}$ and $0.03 \frac{\text{m}}{\text{s}}$ by $A = 20000 \frac{\text{Pa}}{\text{m/s}}$. Test-calculation at $= 13553 \frac{\text{Pa}}{\text{m/s}}$, which is the slope of the curve at $0 \frac{\text{m}}{\text{s}}$, have shown minor differences in the global tendency. Nevertheless the value of $20000 \frac{\text{Pa}}{\text{m/s}}$ should be more accurate and is consequently chosen in the following.

4. RESULTS

For the chosen realistic distances of the orifices, homogeneously small suction velocities are calculated along the porous wall. Variations are shown for different duct pressures and different tap-distances.

For all inviscid calculations, the variation of the pressure inside the chambers is less than 0.08% related to the average chamber pressure.

4.1. Inviscid simulations

The geometrical data as well as the flow conditions are taken from the experiments within the scope of the VER²SUS experiments. In the following, results for the three chosen geometries and pressure-ratios (see TAB 1) are presented.

The fact of nearly zero velocities inside the chambers has to be pointed out, so the streamlines in the calculated flow-field don't represent vortices in the classical sense, but structures in a very slowly moving fluid.

Due to these extremely small velocities in the chamber, and the approximately 100 times smaller values inside the duct, visibly closed streamlines won't be called recirculation-regions or vortices but flow-structures in the following.

4.1.1. Case1

The external pressure for this test-case is chosen by 100500 Pa at a Duct pressure of 99250 Pa and a

distance between the orifices of $2 \cdot 0.125 \text{ m}$ (top picture of FIGURE 7).

The resulting pressure-distribution in the suction-chamber and the suction-velocity along the wall is shown in FIGURE 7. The pressure-variation along the porous wall is nearly constant between 146.54 Pa and 146.51 Pa, a variation of less than 0.03%. The suction-velocity of about 0.0069 m/s varies in the same range for this test-case, which is equivalent with $\Delta v_{suction} \approx 4 \frac{\mu\text{m}}{\text{s}}$.

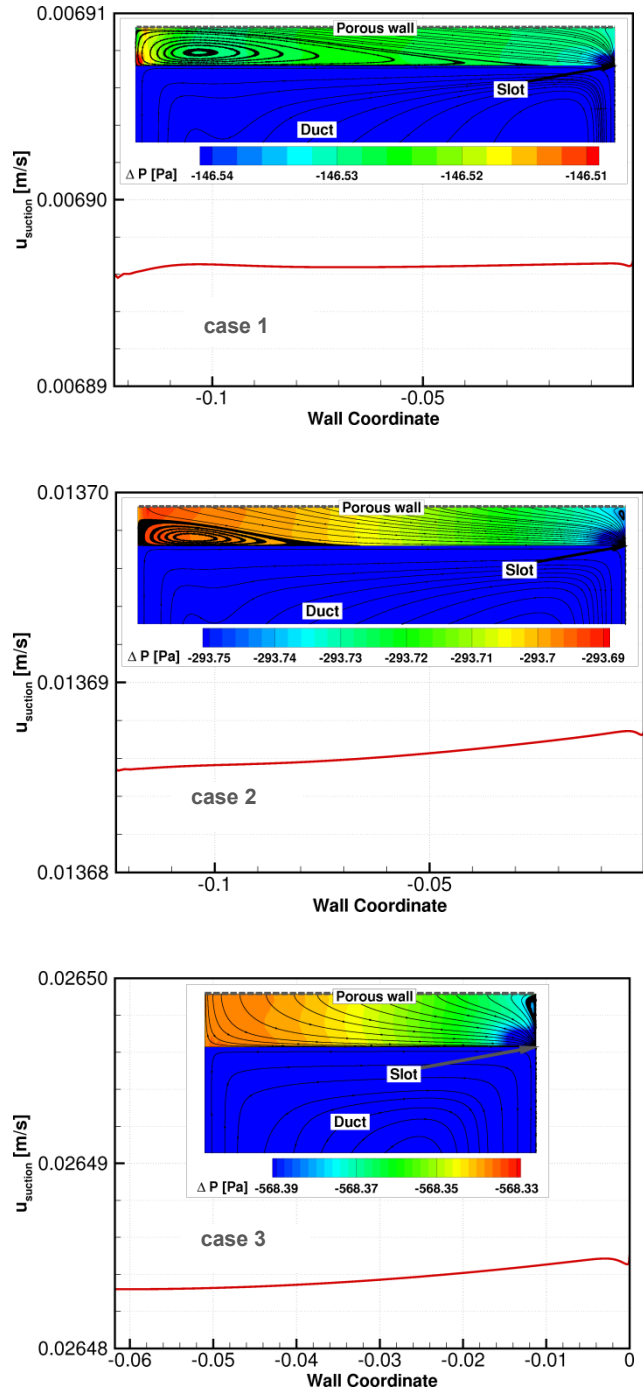


FIGURE 7. Velocity distribution along porous panel wall and pressure inside the chambers.

Such a structure of closed stream-lines appears inside the chamber between symmetry-plane and suction-slot due to the slip-wall condition that allows tangential velocity components along the porous wall. This structure is responsible for the velocity-maximum at the wall coordinate -0.11m.

4.1.2. Case 2

For the second test-case the external pressure is reduced to 99500 Pa at a duct pressure of 95000 Pa. The distance between the orifices is again 0.25 m with the same slot-diameter (middle picture of FIGURE 7).

Closed stream-lines appear in the chamber as well, but the region of this structure is significantly reduced which is a result of the larger pressure-ratio between duct and porous-wall pressure. No local maximum of the suction velocity is visible in contrast to case 1.

Δp inside the chamber is nearly constant in a range between 293.69 Pa and 293.75 Pa which is a slightly larger dimensional difference than in case 1 while the relative variation is kept similar below values of 0.03% due to the increased average pressure.

4.1.3. Case 3

This is a variation of the orifice-period. The number of slots is doubled and consequently the domain-size is cut into halves. External and duct pressure are the same as in case 2, the slot-size is fitted to the constant hole-diameter of 3mm.

Since the geometry of the chamber fits better to the flow inside, closed streamlines do not appear any more, and the suction velocity shows no maximum apart from the suction slot. A very small region with closed stream-lines is visible in the top-left corner of the chamber. These little flow-structures appear also in case 2.

Another outcome of the doubled orifice-number is the pressure difference in the chamber which is nearly doubled in comparison with case 2. It is found in a range between 568.33 Pa and 568.39 Pa. The relative variation is even smaller than in case 2: about 0.02%.

4.2. Navier-Stokes simulation

A viscous calculation for case 2, which is a good representation of the foreseen experiments, is demonstrated in this section. A refined grid for the non-slip boundary condition is generated to resolve the boundary-layer and the flow through the suction slot.

For a nominal unit Reynolds-number of $7 \cdot 10^6 \text{ 1/m}$, the simulations have shown similar small velocities inside the chamber as already demonstrated for the inviscid case. The flow between the inner walls of the chamber consequently gets a very small representative unit Reynolds-number of about 1400 1/m . For this reason only laminar flow is expected inside the chamber.

Chamber- as well as duct walls are defined by non-slip boundary condition, though the boundary-layer influence in the duct is expected to be negligible.

Numerically, convergence over more than 8 orders of magnitude is necessary until the final flow-field is established. Due to the strong gradients near the suction slot and the very small pressure and velocity variation at

the porous wall, this is not an unexpected result if the reduced time-steps for the small near-wall cells of the refined grid are kept in mind.

The vanishing tangential velocity-component at the porous wall results in perpendicular streamlines at this boundary-layer edge, dominated by the suction-velocities. For this reason no more closed streamlines appear in the chamber and each part of the flow is directed towards the slot without any detour.

Comparable pressure- and velocity distributions as in the inviscid case 2 are predicted by this calculation. Even velocities in the slot region are in the same range.

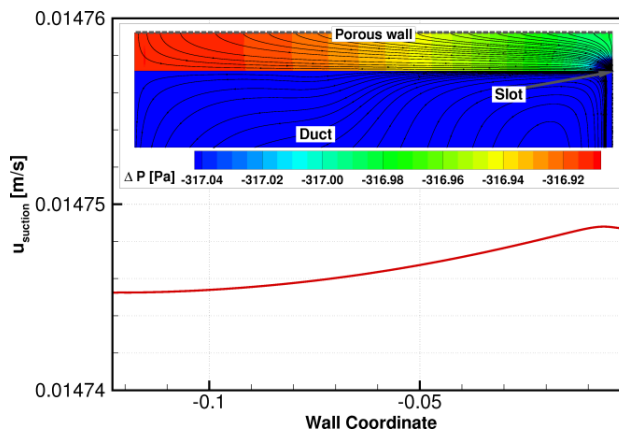


FIGURE 8. Velocity distribution along porous panel wall and difference pressure inside the chamber by a Navier-Stokes simulation of case 2.

5. CONCLUSION

For a simplified suction chamber concept for hybrid laminar flow control by boundary-layer suction, the 2D flowfield inside the chambers is simulated. Within the current study, CFD simulations of the flow inside different geometries are carried out by the DLR FLOWer code to predict velocity as well as pressure distribution behind the porous sheet. Variations of the suction pressure and the tap-distance are carried out for inviscid as well as viscous flow. The suction through the micro-porous surface is approximated by a flux boundary condition, using an analytic relation between difference-pressure and suction velocity at the wall.

The results show very small variations of the relevant flow data like suction velocity and chamber pressure. Both are nearly constant for the investigated geometries by simulating inviscid as well as viscous flow, while the structure of the flow-field inside the chamber changes if non-slip walls and an inviscid approach are used.

Variations of the difference between external and duct pressure have shown other mean data but very little changes in the variation behavior. This statement holds for a doubling of the orifices along the spanwise direction.

While the results indicate, that the velocity-distribution at the suction-wall can be optimized by adjusting the duct-pressure or the number of orifices, no extensive necessity for such an improvement is technically given.

- [1] R.D. Joslin: Overview of laminar flow control. NASA/TP-1998-208705 1998.
- [2] R. Henke: A320 HLF fin flight tests completed. Air&Space Europe, 1, pp 76-79 1999.
- [3] G. Schrauf, K.H. Horstmann: Simplified hybrid laminar flow control. ECCOMAS 2004, Jyväskylä, Finland, 24-28 July 2004. CD-Proceedings 2004.
- [4] C.-H. Rohardt, A. Seitz, et.al.: Simplified-HLFC/ Entwurf eines Seitenleitwerks mit Hybrid-Laminarhaltung für den Airbus A320. Deutscher Luft- und Raumfahrt Kongress, 27.-29.9.2011, Bremen.
- [5] K.-H. Horstmann, W. Schröder: Simplified Suction System for a HLFC L/E Box of an A320 Fin. ALTTA Technical Report TR 23, 2001.
- [6] S. Enk: Investigation of Boundary Conditions for the Simulation of Suction by Hybrid Laminar Flow. Deutscher Luft- und Raumfahrt Kongress, 10.-12.9.2013, Stuttgart.
- [7] N. Kroll, C.C. Rossow, D. Schwamborn, K. Becker and K. Heller: Megaflow – a Numerical Flow Simulation Tool for Transport Aircraft Design. ICAS 2002 Congress, 2002.